

Review

Recent Progress in Atomic-Level Understanding of Cu/SSZ-13 Selective Catalytic Reduction Catalysts

Feng Gao *  and Charles H. F. Peden * 

Institute for Integrated Catalysis, Pacific Northwest National Laboratory, Richland, WA 99352, USA

* Correspondence: feng.gao@pnnl.gov (F.G.); chuck.peden@pnnl.gov (C.H.F.P.)

Received: 2 March 2018; Accepted: 28 March 2018; Published: 31 March 2018



Abstract: Cu/SSZ-13 Selective Catalytic Reduction (SCR) catalysts have been extensively studied for the past five-plus years. New and exciting fundamental and applied science has appeared in the literature quite frequently over this time. In this short review, a few topics specifically focused on a molecular-level understanding of this catalyst are summarized: (1) The nature of the active sites and, in particular, their transformations under varying reaction conditions that include dehydration, the presence of the various SCR reactants and hydrothermal aging; (2) Discussions of standard and fast SCR reaction mechanisms. Considerable progress has been made, especially in the last couple of years, on standard SCR mechanisms. In contrast, mechanisms for fast SCR are much less understood. Possible reaction paths are hypothesized for this latter case to stimulate further investigations; (3) Discussions of rational catalyst design based on new knowledge obtained regarding catalyst stability, overall catalytic performance and mechanistic catalytic chemistry.

Keywords: selective catalytic reduction (SCR); zeolite; Cu/SSZ-13; reaction mechanisms; hydrothermal stability; standard SCR; fast SCR

1. Introduction

The discovery [1–4] and the rapid commercialization shortly thereafter, of Cu/SSZ-13 as a selective catalytic reduction (SCR) catalyst for NO_x abatement for the transportation industry, has been one of the most exciting milestones in environmental catalysis in recent years [5–9]. Inspired by this and also by the fact that SSZ-13 itself [10], a Chabazite silica-alumina zeolite, offers great structural simplicity for basic research, there has been an exponential growth in the number of published studies of Cu/SSZ-13 appearing in the open literature in recent years. In particular, Figure 1 depicts the numbers of papers published each year for the past 8 years containing “Cu”, “SSZ-13” and “SCR” in their contents, using the “Web of Science” search engine. Notably, ~180 papers, with total citations greater than 4000, have been published in this short period of time. While likely an incomplete search particularly for 2017, these numbers clearly reflect the importance, popularity and enthusiasm for research of the now commercialized Cu/SSZ-13 catalyst. For comparison, from 1970 to 1980, during which time the three-way catalyst was developed and commercialized, fewer than 30 publications appeared in the open literature addressing “emission control catalyst,” searched using the same engine.

In 2015, we published the first comprehensive review of the early understandings of Cu/SSZ-13 catalyst regarding its synthesis, structural details from spectroscopy and theory, SCR kinetics, as well as key aspects of the catalyst for practical applications [6]. Now after 3 years, new and exciting results have appeared in literature, especially with respect to the developing molecular-level understanding of the nature of the active Cu species under realistic operating (i.e., situ/operando) conditions, as well as the SCR reaction mechanisms [11–26]. As such, it seems timely to review these new fundamental understandings. We note, however, that this is not a comprehensive review but a summary of selected topics; in particular, topics relevant for the molecular-level understanding about the nature

of Cu and the SCR reaction mechanisms. More specifically, we summarize very recent results on the mechanistic relevance of a binuclear Cu complex formed from mobile mononuclear complexes and how identification of several catalytically active Cu species led to an understanding of critical rate-limiting steps of reaction (Section 3). To do so, we also need to first briefly review what is now known about the multiple forms of Cu species present under various conditions of temperature and gas-phase composition (Section 2). Because the forms of Cu present also effect another critical aspect of these catalysts for practical applications, notably their stability, we also summarize some recent studies aimed at identifying optimum catalysts for both reactivity and stability in Section 4.

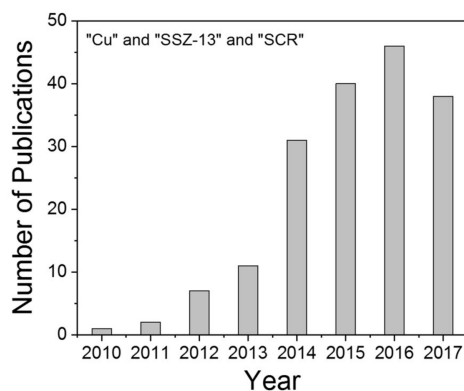


Figure 1. Number of recent publications on Cu/SSZ-13 catalysts for NH₃ Selective Catalytic Reduction (SCR).

2. Transformations of Cu Active Species

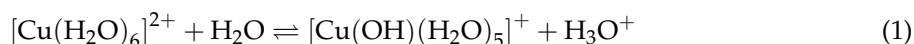
Cu/SSZ-13 is typically prepared via solution ion-exchange of NH₄/SSZ-13 with Cu salts at low pHs to avoid Cu agglomeration, or by so-called one-pot synthesis methods [27–31]. Unless Cu is present at levels exceeding the ion-exchange capacities of the particular SSZ-13 composition used, the current general consensus is that, in the freshly prepared specimens, Cu is present as isolated ions, including Cu²⁺ balanced by two nearby framework negative charges (abbreviated as Cu²⁺-2Z, where Z represents a charged zeolite framework site) and a [Cu(OH)]⁺ species balanced by one framework negative charge (as [Cu(OH)]⁺-Z) [17,31–33]. It is also generally agreed, based on almost identical X-ray absorption near edge structure (XANES) spectra with model Cu salt solutions, that these ions are fully solvated as [Cu(H₂O)₆]²⁺ and [Cu(OH)(H₂O)₅]⁺ complexes in hydrated ambient samples [20,34,35]. These two ions are, for practical purposes, spectroscopically indistinguishable and they reside in the Chabazite (CHA) cages where they have relatively small (i.e., longer range) interactions with the CHA framework. Starting from this hydrated state, three scenarios are described next regarding the transformations of these Cu species due to the following changing conditions: (1) dehydration in vacuum or an inert gas; (2) hydrothermal aging (HTA); or (3) exposure to NH₃, including that occurring during low-temperature SCR reaction conditions.

2.1. Dehydration

During dehydration, complete H₂O desorption occurs between ~250–300 °C depending somewhat on the specific dehydration conditions. With the removal of H₂O ligands, Cu ions now migrate to cationic exchange positions and bond to lattice O (O_L) of the zeolite framework. Such a change is well reflected by changes in unit cell parameters of the CHA substrate from X-ray diffraction (XRD) [27,35], -OH and H₂O vibrations from FTIR [35], X-ray absorption and emission spectra (XAS and XES) [20] and hyperfine interactions between the unpaired electron and the nuclear spin of Cu(II) (I = 3/2) from electron paramagnetic resonance (EPR) [36]. It is now well-documented that in dehydrated Cu/SSZ-13, Cu²⁺-2Z with Cu ions located in windows of 6-membered rings (6 MR) are the energetically most

favorable configuration. As such, Schneider and coworkers predicted that exchanged Cu^{2+} ions first saturate these 2Al sites before populating unpaired, or 1Al, sites as $[\text{Cu}(\text{OH})]^{+}$ [17]. Note that the relative populations of Cu^{2+} -2Z and $[\text{Cu}(\text{OH})]^{+}$ -Z are dependent both on Si/Al and Cu/Al ratios of the Cu/SSZ-13 material, as shown in Figure 2.

This prediction, originated primarily from thermodynamics grounds, does not rigorously describe actual Cu/SSZ-13 catalyst compositions. In particular, a number of studies discovered that $[\text{Cu}(\text{OH})]^{+}$ -Z can populate before Cu^{2+} -2Z saturation [18,20,37]. A likely explanation is that, in fully hydrated samples, dynamic equilibrium exists between $[\text{Cu}(\text{H}_2\text{O})_6]^{2+}$ and $[\text{Cu}(\text{OH})(\text{H}_2\text{O})_5]^{+}$ ions that can be described using Reaction (1):



Then, depending critically on the composition (Si/Al and Cu/Al ratios), specific Cu distributions and how dehydration is carried out, $[\text{Cu}(\text{OH})]^{+}$ -Z can very well be kinetically stabilized in the dehydrated form. For example, Martini et al. very recently demonstrated that a Cu/SSZ-13 sample with Si/Al = 14 and Cu/Al = 0.1 can contain substantial amounts of $[\text{Cu}(\text{OH})]^{+}$ -Z as determined with XANES [20], even though all of the Cu ions can, in principle, be more thermodynamically stabilized as Cu^{2+} -2Z (Figure 2).

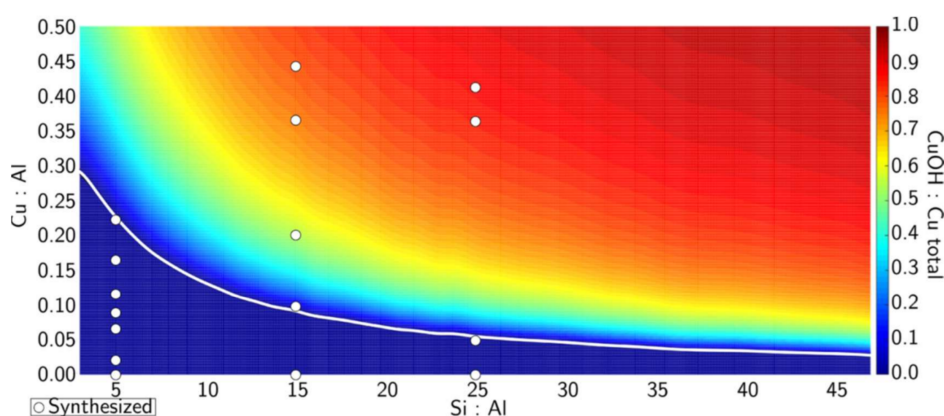


Figure 2. The predicted Cu site compositional phase diagram versus Si:Al and Cu:Al ratios, with the color scale indicating predicted fractions of CuOH. The white line demarcates the transition from a [Z2-CuII]-only region to a mixed [Z2-CuII]/[Z-CuII-OH] region. White circles indicate compositions of synthesized Cu-SSZ-13 samples used to verify the computed predictions. Reprinted with permission from *J. Am. Chem. Soc.*, 2016, 138, 6028–6048. Copyright 2016, American Chemical Society.

Even though $[\text{Cu}(\text{H}_2\text{O})_6]^{2+}$ and $[\text{Cu}(\text{OH})(\text{H}_2\text{O})_5]^{+}$ ions are likely spectroscopically indistinguishable by XANES, indirect evidence does exist for the reversible reaction described in Reaction (1) from electron paramagnetic resonance (EPR) measurements. Figure 3 presents EPR spectra collected during dehydration of a Cu/SSZ-13 sample with Si/Al = 6 and Cu/Al = 0.032 [38]. At such Al abundance and low Cu loadings, it is expected that $[\text{Cu}(\text{H}_2\text{O})_6]^{2+}$ is the only Cu species in the hydrated form and it will be converted exclusively to Cu^{2+} -2Z upon dehydration. However, at intermediate dehydration temperatures (e.g., 150 °C), the clear signal intensity loss suggests formation of EPR silent $[\text{Cu}(\text{OH})]^{+}$ [36], even though it eventually converts to EPR active Cu^{2+} -2Z as evidenced by the signal intensity recovery at higher temperatures. For catalysts with higher Si/Al and Cu/Al ratios, $[\text{Cu}(\text{OH})]^{+}$ -Z can indeed be thermodynamically stabilized during dehydration.

Another interesting Cu ion transformation during dehydration is the so-called “auto-reduction”; that is, formation of Cu(I) moieties in vacuum or in an inert gas flow without addition of reductants [36]. Although not conclusive, a likely mechanism can be described as follows, involving formation of an OH radical:



It is also notable that auto-reduction even occurs in the presence of O_2 , as long as the temperature is high enough [25,31]. Applying multivariate curve resolution (MCR) techniques to XANES linear combination fit (LCF) analysis, Martini et al. [20] recently studied dehydration of a series of Cu/SSZ-13 materials with varying compositions. Using 5 model structures, detailed Cu transformations as a function of temperature were quantified and the results are shown in Figure 4. Besides the expected result that lower Si/Al ratios favor Cu^{2+} -2Z population, the authors also discovered that the extents of autoreduction are the highest at intermediate Si/Al ratios, which they rationalized as due to autoreduction proceeding through a cooperative multi-step process involving proximal acid sites. However, this conclusion is in contrast to H_2 temperature-programmed reduction (H_2 -TPR) results by Gao et al. [31], who demonstrated, based on H_2 consumption differences between ambient and autoreduced samples, that the extent of autoreduction increases with increasing Si/Al ratios at similar Cu/Al ratios. Besides the well-known positioning for Cu^{2+} -2Z and $[\text{Cu}(\text{OH})]^+$ -Z in dehydrated Cu/SSZ-13, N_2 adsorption FTIR measurements by Martini et al. [20] suggest that autoreduced Cu ions (i.e., Cu^+ -Z) occupy both windows of 6 MRs and 8 MRs, with relative populations that depend on Cu/Al and Si/Al ratios.

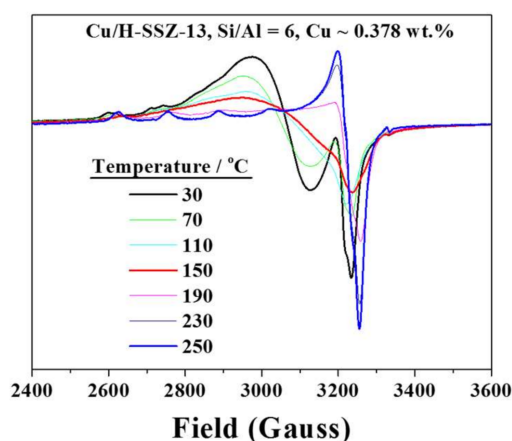
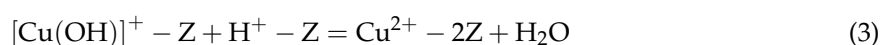


Figure 3. Electron Paramagnetic Resonance (EPR) spectra of a Cu/SSZ-13 sample (Si/Al = 6, Cu/Al = 0.032) during dehydration. Reprinted from *J. Catal.*, 2014, 319, 1–14. Copyright 2014, with permission from Elsevier.

2.2. Hydrothermal Aging

Hydrothermal stability of Cu/SSZ-13 is a critical criterion for its practical applications; as such, hydrothermal aging effects have been extensively addressed [29,37,39–41]. Hydrothermal stability depends on various parameters including catalyst composition, aging temperature and duration. Typically, aging at ~ 700 °C and lower causes limited structural degradation of Cu/SSZ-13 (e.g., dealumination, surface area loss), while higher aging temperatures induce partial to even complete structural damage [37,41].

Recently, Luo et al. [18] hydrothermally aged a state-of-the-art commercial Cu/SSZ-13 catalyst with Si/Al = 9.5 and Cu/Al = 0.3 at 600 °C for varying durations from 1 to 100 h. Subsequently, NH_3 temperature-programmed desorption (NH_3 -TPD, following NH_3 adsorption at 150 °C) was performed and the results are shown in Figure 5. The TPD feature above 400 °C is due to NH_3 desorption from Brønsted acid sites, while the feature below 300 °C is attributed to NH_3 desorption from Cu. Note that the aging temperature of 600 °C causes essentially no dealumination as determined from ^{27}Al NMR; as such, Brønsted acidity loss during aging is presumed to be caused by the reverse of Reaction (1):



This notion is fully consistent with NH_3/Cu ratio quantifications using the TPD data, where it was found that, at an NH_3 adsorption temperature 150°C , ~ 2 molecules of NH_3 adsorb on $\text{Cu}^{2+}\text{-Z}$ and ~ 1 molecule of NH_3 adsorb on $[\text{Cu}(\text{OH})]^+\text{-Z}$. The fact that 1 molecule of NH_3 adsorbs on 1 Brønsted acid site nicely explains the largely invariant NH_3 yields as a function of aging time that are evident in Figure 5. Two key additional points are worth noting for this study. First, even though $[\text{Cu}(\text{OH})]^+\text{-Z}$ can be kinetically stabilized prior to $\text{Cu}^{2+}\text{-Z}$ saturation in freshly prepared catalysts, given enough time and thermal energy during hydrothermal aging, $[\text{Cu}(\text{OH})]^+\text{-Z}$ will convert to the thermodynamically more stable $\text{Cu}^{2+}\text{-Z}$ species. Second, although NH_3 can fully solvate $\text{Cu}^{2+}\text{-Z}$, forming a detached $[\text{Cu}(\text{NH}_3)_4]^{2+}$ complex at ambient temperatures, at higher temperatures, Cu(II) sites interacting with both lattice O (O_L) and NH_3 (e.g., as partially solvated $[\text{Cu}(\text{O}_\text{L})_2(\text{NH}_3)_2]^{2+}$) appear to better describe these species. More details on Cu and NH_3 interactions will be given below.

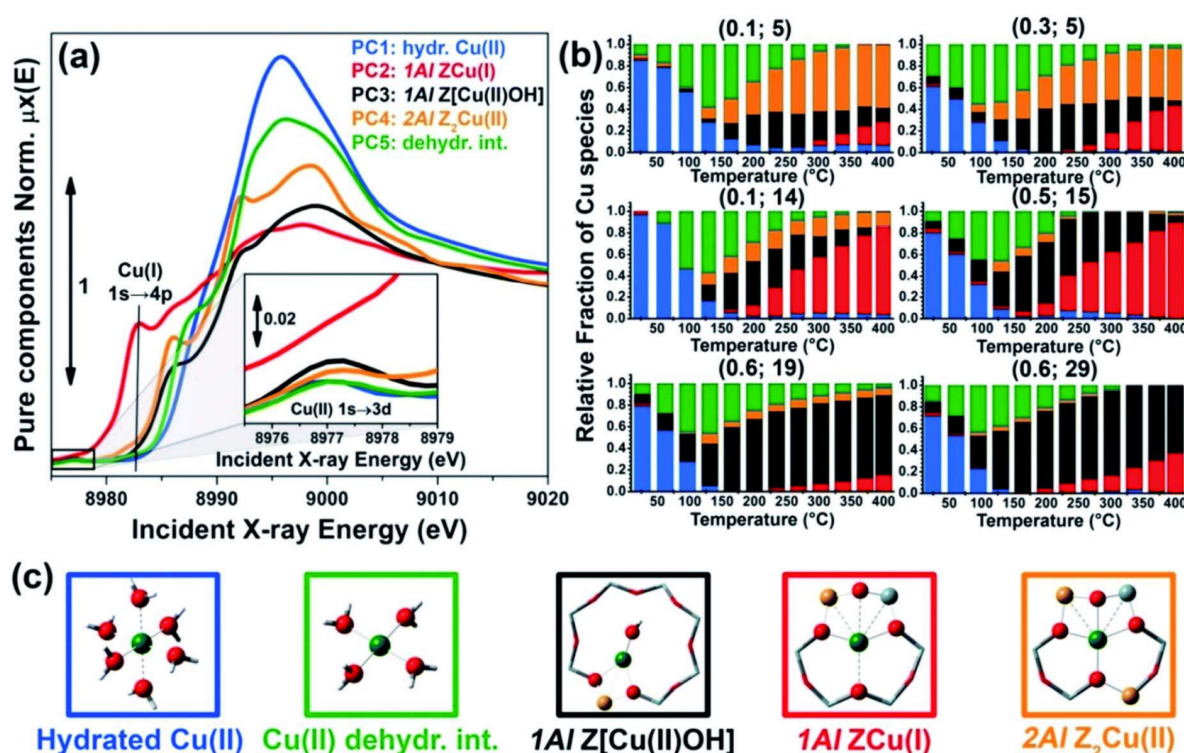


Figure 4. Multivariate curve resolution (MCR) coupled with the alternating least square (ALS) analysis of global temperature-dependent XANES dataset collected for six Cu-CHA samples with different compositions during He-activation from 25 to 400°C , assuming the presence of 5 pure components. (a) XANES spectra of pure components $\mu_i(E)$ derived from MCR-ALS. The inset reports a magnification of the Cu(II) $1s \rightarrow 3d$ transition region in the theoretical spectra; (b) Temperature-dependent abundance of pure species, $w_i^p(\text{Cu}/\text{Al}; \text{Si}/\text{Al}, T)$, in each of the catalysts (bars have the same colors as the corresponding spectra in panel (a)); (c) Proposed assignment of the five pure components (PC) to specific Cu-species/sites formed in the Cu-CHA catalyst as a function of composition and activation temperature, using the same color code as in parts (a) and (b); Blue (PC1): mobile Cu(II)-aquo-complexes $[\text{Cu}(\text{II})(\text{H}_2\text{O})_n]^{2+}/[\text{Cu}(\text{II})(\text{H}_2\text{O})_{n-1}(\text{OH})]^+$ with $n = 6$; green (PC5): Cu(II) dehydration intermediate, possibly represented by mobile $[\text{Cu}(\text{II})(\text{H}_2\text{O})_n]^{2+}/[\text{Cu}(\text{II})(\text{H}_2\text{O})_{n-1}(\text{OH})]^+$ complexes with $n = 4$; black (PC3): 1Al Z[Cu(II)-OH] sites in their oxidized form; red (PC2): 1Al Z-Cu(I) sites in their reduced form, resulting from self-reduction of 1Al Z[Cu(II)OH] species; orange (PC4): 2Al Z₂-Cu(II) sites. Atom color code: Cu: green; H: white; O: red; Si: grey; Al: yellow. *Chem. Sci.*, **2017**, *8*, 6836–6851—Published by The Royal Society of Chemistry.

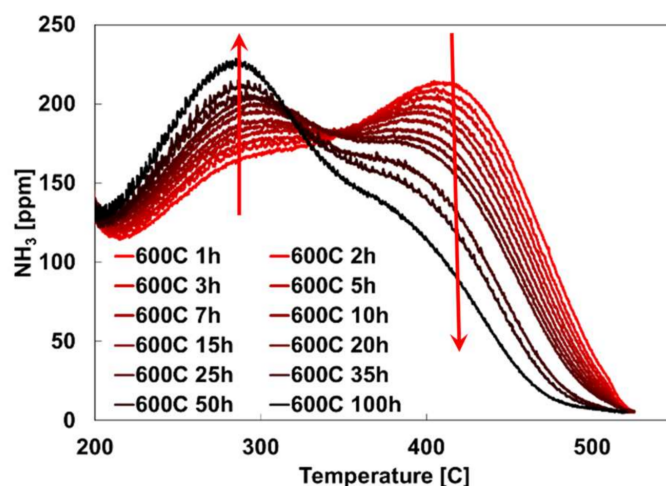


Figure 5. NH_3 -TPD profiles for Cu/SSZ-13 upon progressive aging at 600 °C; arrows indicate increasing aging times. Reprinted from *J. Catal.*, **2017**, *348*, 291–299. Copyright 2017, with permission from Elsevier.

Hydrothermal aging under more harsh conditions can cause additional types of Cu transformations, including especially formation of copper oxide clusters (CuO_x). Song et al. [37] recently conducted detailed aging studies of a Cu/SSZ-13 catalyst with Si/Al = 12 and Cu loading 2.1 wt % (corresponding to Cu/Al = 0.25), where aging temperatures systematically varied from 550 to 900 °C. The fresh and aged samples were examined with EPR in both hydrated and dehydrated forms at cryogenic temperatures in order to quantify Cu^{2+} -2Z, $[\text{Cu}(\text{OH})]^+$ -Z and CuO_x clusters in these samples, based on the facts that Cu^{2+} -2Z is EPR active in both hydrated (i.e., as $[\text{Cu}(\text{H}_2\text{O})_6]^{2+}$) and dehydrated forms, CuO_x clusters are always EPR silent due to antiferromagnetic effects and $[\text{Cu}(\text{OH})]^+$ -Z is EPR active when hydrated (as $[\text{Cu}(\text{OH})(\text{H}_2\text{O})_5]^+$) but becomes EPR silent when dehydrated due to pseudo Jahn-Teller effects [36]; that is, absorbed microwave energy by $[\text{Cu}(\text{OH})]^+$ -Z dissipates too rapidly for the time scale of EPR measurements.

From the results shown in Figure 6, $[\text{Cu}(\text{OH})]^+$ -Z content monotonically decreases while CuO_x content increases with increasing aging temperature. Cu^{2+} -2Z content first increases, reaching its highest amount of ~1.5 wt % in the sample aged at 700 °C and then declines slightly before stabilizing at ~1.2 wt % at higher aging temperatures. From such quantifications, it is evident that $[\text{Cu}(\text{OH})]^+$ -Z species primarily convert to Cu^{2+} -2Z and perhaps a portion to CuO_x clusters at aging temperatures ≤ 700 °C. The former transformation, as described by Reaction (3), is also found for the current state-of-the-art commercial Cu/SSZ-13 catalyst (Figure 5) [18]. At aging temperatures of 750 °C and above, Cu^{2+} -2Z stabilizes at ~1.2 wt % indicating that this portion of Cu^{2+} must be located in windows of 6MRs with paired Al sites; that is, at the energetically most stable locations for Cu^{2+} -2Z [33]. The remaining Cu^{2+} species are less stable, ultimately converting to CuO_x at higher aging temperatures. An important outcome of this result is the remarkable hydrothermal stability evident for Cu^{2+} -2Z located in windows of SSZ-13 6 MRs, where they survive even under extremely harsh hydrothermal aging temperatures of 900 °C. On the other hand, $[\text{Cu}(\text{OH})]^+$ -Z is hydrothermally much less stable; some of which converts to more stable Cu^{2+} -2Z and the rest to CuO_x clusters during aging.

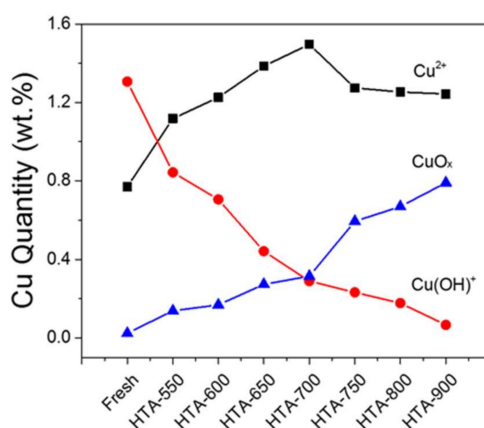
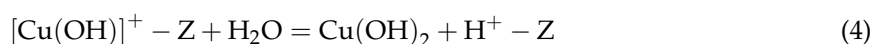


Figure 6. Estimation of Cu²⁺, Cu(OH)⁺ and CuO_x in fresh and hydrothermally aged Cu/SSZ-13 samples with Si/Al = 12 and Cu/Al = 0.25. HTA represents hydrothermal aging. Reprinted with permission from *ACS Catal.*, 2017, 7, 8214–8227. Copyright 2017, American Chemical Society.

The processes by which [Cu(OH)]⁺-Z converts to CuO_x clusters are not apparent at present. Song et al. [37] proposed recently that [Cu(OH)]⁺-Z first undergoes a hydrolysis reaction to form mobile Cu(OH)₂ (Reaction (4)) during hydrothermal aging, with the latter then migrating and agglomerating, to eventually form CuO_x clusters.



Hydrolysis activation barriers simulated from DFT are fully consistent with the hydrothermal stability difference between [Cu(OH)]⁺-Z and Cu²⁺-2Z, where it was found that the former hydrolyzes more readily than the latter.

The nature of the CuO_x clusters formed during hydrothermal aging, for example, their sizes, locations and whether they incorporate any aluminum (from zeolite substrate dealumination), is also essentially unknown at present due, in part, to a lack of techniques for their unambiguous characterization. For example, using scanning TEM, Song et al. [37] failed to identify clusters that can be assigned to CuO_x in aged Cu/SSZ-13. Notable also is that a lack of surface Al and Cu segregation evident from XPS analyses indicates that these moieties may still be located in pores and channels of SSZ-13. Weckhuysen and coworkers [22] recently utilized atom probe tomography (APT) to compare aged Cu/ZSM-5 and Cu/SSZ-13. In Cu/ZSM-5, severe Cu and Al aggregation was demonstrated and mapped in 3D and a Cu/Al atomic ratio of ~2 for the aggregates indicates formation of copper aluminate. Similarly, irreversible formation of a Cu-Al phase was confirmed via XAFS measurements in a study by Vennestrøm et al. [42] for aged Cu/ZSM-5. In both studies, a phase similar to CuAl₂O₄ spinel was suggested. However, formation of a crystalline spinel phase is likely to be difficult in the confined spaces of zeolite channels and cages. Instead, formation of distorted amorphous phases with stoichiometry perhaps close to that of CuAl₂O₄ spinel may better describe the Cu-Al phases formed in aged Cu/ZSM-5. In contrast, APT analysis of aged Cu/SSZ-13 shows some Cu and Al clustering but to a limited degree (relative to Cu/ZSM-5) with undetermined stoichiometries [22]. It can be concluded, therefore, that CuO_x formed in aged Cu/SSZ-13 can indeed interact with Al from substrate dealumination but stoichiometries and structures of the thus formed species are still undetermined.

2.3. Interactions with NH₃

In comparison to NO_x and H₂O, interactions between Cu ions and NH₃ are much stronger; this renders a generally agreed scenario that, under low-temperature NH₃-SCR reaction conditions, Cu-NH₃ complexes are abundant and some of these are key intermediates for reaction [15,17,20]. Therefore, it is of considerable relevance to study species formed by adsorption of NH₃ on Cu/SSZ-13

and identify their mechanistic involvement in NH₃-SCR. Cu-NH₃ interactions are dependent on nature of Cu ions (Cu²⁺, [Cu(OH)]⁺ or Cu⁺), local environments of these Cu ions, gas-phase compositions and temperature.

Schneider and coworkers [17] utilized DFT thermodynamic screening to predict species that are likely relevant to NH₃-SCR; that is, in the presence of 300 ppm NH₃, 2% H₂O and varying O₂ pressures as a function of temperature. From the results shown in Figure 7, Cu²⁺-Z and [Cu(OH)]⁺-Z display completely different reactivity toward NH₃, where the latter is much more readily reducible to Cu⁺-Z by NH₃. Under low-temperature (e.g., 200 °C) SCR conditions, this simulation predicts a dominance of [Cu(NH₃)₄]²⁺, [Cu(OH)(NH₃)₃]⁺ and [Cu(NH₃)₂]⁺ species, all of which detach from the SSZ-13 framework as mobile species [17]. Among these, [Cu(NH₃)₂]⁺ has the highest mobility and can readily pass through 8MR openings that are shared by neighboring unit cells. Note that, while the studies discussed above by Luo et al. [18] demonstrate via NH₃-TPD that likely Cu-NH₃ complexes are [Cu(O_L)₂(NH₃)₂]²⁺ and [Cu(O_L)₂(OH)(NH₃)]⁺ following NH₃ adsorption and purging at 150 °C, the apparent discrepancy can be understood from the gas-phase NH₃ pressure differences, where the presence of gas phase NH₃ allows for higher coordination with NH₃ ligands.

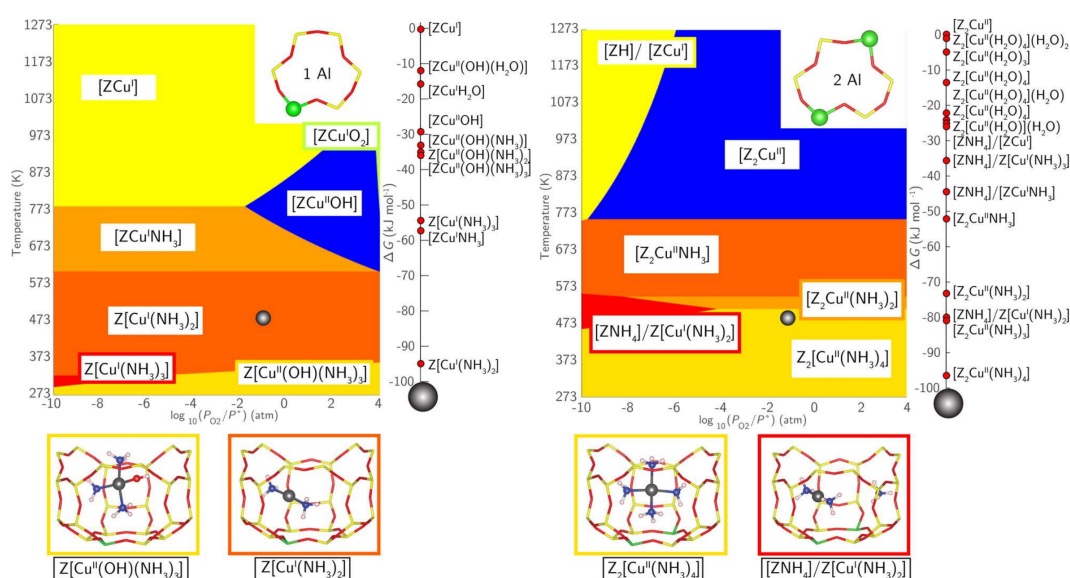


Figure 7. Phase diagrams for 1Al (left) and 2Al (right) sites with varying T and PO₂ at 300 ppm of NH₃ and 2% H₂O. Relative rankings for all stable species—ΔG_{form} < 0 at 473 K and 10% O₂ (chrome spheres on the phase diagrams)—are given to the right of each phase diagram. The structures shown on the bottom are the most stable CuI (red outline) and CuII (golden outline) species under these conditions. Reprinted with permission from *J. Am. Chem. Soc.*, 2016, 138, 6028–6048. Copyright 2016, American Chemical Society.

EPR can be used to characterize Cu(II)-NH₃ complexes in a quantitative way. An added benefit of this technique is that Cu(I)-NH₃ complexes, being EPR silent, do not complicate the measurements. As shown by the spectra in Figure 8, obtained subsequent to NH₃ and ¹⁵NH₃ adsorption on a one-pot synthesized Cu/SSZ-13 followed by degassing at 25 °C, second derivatives of the EPR signals display super-hyperfine structures that can be used to determine Cu(II)-NH₃ coordination [14]. The super-hyperfine structures come from interactions of the Cu(II) unpaired electron with the nuclear spin of ¹⁴N (I = 1) or ¹⁵N (I = 1/2), which splits the EPR lines into 2nI + 1 components, where I is the nuclear spin and n is the number of nuclei. Based on this, species B in Figure 8 can be assigned to [Cu(NH₃)₅]²⁺ and species C to [Cu(O_L)₂(NH₃)₂]²⁺ [14]. The former complex is not stable at higher temperatures, where it loses NH₃ ligands sequentially with increasing temperature. Possible structures that form in this process were simulated with DFT [14].

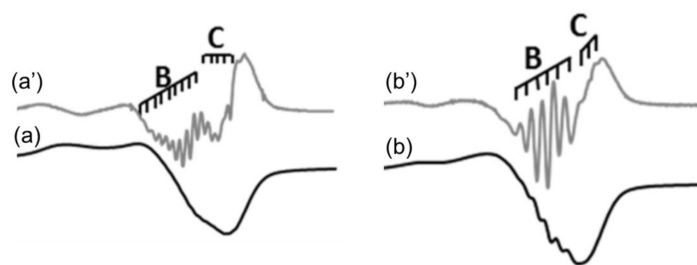


Figure 8. EPR spectra recorded at 25 °C after the adsorption of 6 NH₃/Cu atom (a) or 6 ¹⁵NH₃ per Cu (b) on Cu-SSZ-13 followed by degassing at 25 °C. (a' and b') are second derivatives of the spectra, used to determine the super-hyperfine structure of EPR signals B and C. Reprinted with permission from *J. Phys. Chem. Lett.*, 2015, 6, 1011–1017. Copyright 2015, American Chemical Society.

It is now well established that NH₃ itself can reduce Cu(II) to Cu(I) [17,43]. In particular, the theoretical phase diagrams shown in Figure 7 indicate that [Cu(OH)]⁺ is readily reduced at low temperatures irrespective of the O₂ pressure. In the absence of NH₃ complexation, Cu²⁺ reduction is more difficult, requiring higher temperatures and low O₂ pressures. Experimentally, it has been shown that EPR signals disappear almost completely by heating NH₃ saturated Cu/SSZ-13 to 250 °C, demonstrating formation of EPR silent Cu(I) moieties [14]. A sharp Cu K-edge feature at 8982.5 eV, characteristic for Cu(I) upon NH₃ introduction as probed with XANES also clearly indicates Cu(II) reduction to Cu(I) [20,44]. Based on XAS and XES experimental findings, prior literature assignments and DFT simulations, Giordanino et al. first proposed that these Cu(I) moieties are O_L-Cu⁺-NH₃ and NH₃-Cu⁺-NH₃ species and emphasized the linear nature of the latter [43]. Their initial simulated structures are shown in Figure 9, although it is now known that the NH₃-Cu⁺-NH₃ species are much more delocalized in the zeolite than that indicated in the figure.

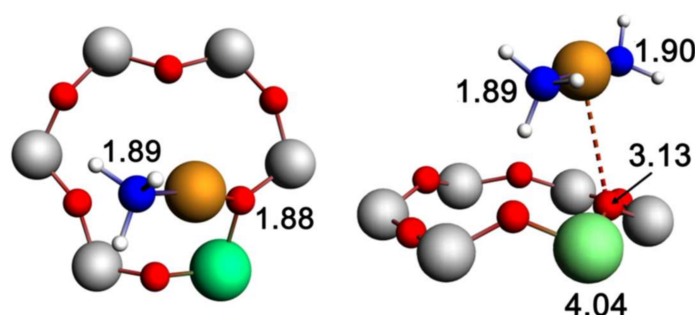
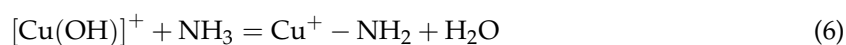


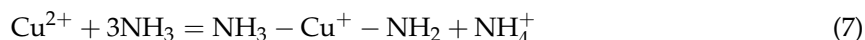
Figure 9. Local Cu environments after adsorption of one (left) and two (right) NH₃ molecules. Color code: orange, Cu; green, Al; gray, Si; red, O; blue, N; white, H. Distances between Cu and neighboring atoms are indicated in angstroms. Reprinted with permission from *J. Phys. Chem. Lett.*, 2014, 5, 1552–1559. Copyright 2014, American Chemical Society.

Detailed reaction mechanisms for Cu(II) reduction to Cu(I) by NH₃ are not understood. Possible reaction pathways are shown as follows:



Reaction (5) has been initially suggested to be energetically unfavorable due to a high activation barrier of +119 kJ/mol from DFT simulations [11]. However, in the presence of surplus NH₃ molecules to provide sufficient solvation effects, energy barriers can drop substantially to 30–34 kJ/mol, making

the process much more feasible [14]. Therefore, a more likely Reaction (5) should be modified to, for example, Reaction (7).



Reaction (6), on the other hand, is expected to require much less NH_3 solvation assistance since H_2O formation is a strong driving force energetically. This may well explain why $[\text{Cu}(\text{OH})]^+$ is much more readily reducible than uncomplexed Cu^{2+} ions [17]. Note, however, that Reactions (5–7) have not been proven experimentally. In particular, the presence of an $-\text{NH}_2$ species has not been demonstrated. Possible reasons are that this species is overwhelmed by the more prevalent NH_3 ligands, or its instability leads to rapid consumption, for example, via formation and decomposition of N_2H_4 [43]. Clearly, more work is needed to gain further details on ‘direct’ Cu(II) ion reduction by NH_3 .

The high mobility for $[\text{Cu}(\text{NH}_3)_2]^+$, as will be shown in the next section, plays a critical role in low-temperature SCR. Of note is that this characteristic is also used to prepare Cu/SSZ-13 using NH_3 -assisted, reaction-driven ion exchange at low temperatures [44,45]. For example, treating Cu_2O and zeolite physical mixtures in NH_3 or $\text{NH}_3 + \text{NO}$ at 250°C effectively converts Cu_2O into Cu ions that are anchored at zeolite ion-exchange sites due to formation, migration and reaction of mobile $[\text{Cu}(\text{NH}_3)_2]^+$ complexes [44].

3. NH_3 -SCR Mechanisms

3.1. Standard NH_3 -SCR

The “Standard” NH_3 -SCR reaction is stoichiometrically shown in Reaction (8):



Complexity of this reaction is clearly evident in the stoichiometry: the reaction is redox in nature and there are 3 reactants to activate. Furthermore, complexity is also evident in the nature of the catalytically active Cu species, as first recognized from SCR kinetics. For example, Figure 10 displays steady state NO_x light-off curve for a Cu/SSZ-13 catalyst with relatively low Cu loading, allowing low- and high-temperature reaction regimes to be clearly resolved [19,38]. Importantly, the NO_x conversion decrease with increasing temperature between ~ 250 and 350°C indicates a temperature-dependent change in the nature of active Cu sites, which has now been repeatedly demonstrated via in situ/operando XAS. In particular, below this temperature range, Cu ions are fully solvated by NH_3 as mobile mono-Cu complexes in SSZ-13 cages, while above 350°C , Cu ions anchor at (complex to) cationic sites of the zeolite framework [15].

In the low-temperature regime, strong Cu loading dependence is found in SCR kinetics. For example, as shown in Figure 11, a linear correlation between SCR rates and Cu loading (i.e., invariant turnover frequencies, TOFs), expected for isolated Cu-ions being the active sites, is only found at intermediate Cu loadings for a series of catalyst samples with essentially only isolated Cu ions [38]. The decrease in TOFs at high Cu loadings can, at least in part, be explained by mass transfer limitations for the reactants. In particular, when Cu loadings are sufficiently high, not all of the Cu ions will be readily accessible to the reactants and, in this way, the ones that are deep in the bulk of the zeolite will be underutilized, causing apparent TOFs to drop. Still, measured reaction activation energies will not decrease in this case, as usually expected from reactant transfer limitations; this is because SCR kinetics will essentially only measure reaction carried out by Cu ions in the outer layers of the catalysts that do not sense such limitations. More significantly, in the low Cu-loading regime, SCR rates also deviate from the linear SCR rate versus Cu loading correlation for completely different reasons. In probing this low Cu-loading regime, critical new insights have been provided for understanding the standard SCR mechanism.

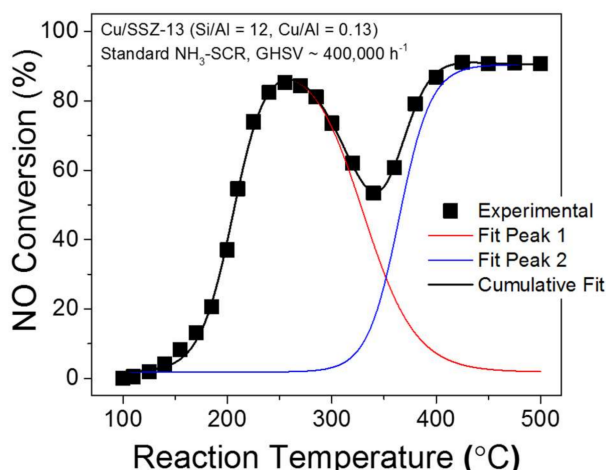


Figure 10. NO conversion versus temperature data (■) for standard SCR over a Cu/SSZ-13 catalyst with Si/Al = 12 and Cu/Al = 0.13. The reactant feed contains 350 ppm NH₃, 350 ppm NO, 14% O₂, 2.5% H₂O balanced with N₂ at a gas hourly space velocity (GHSV) of 400,000 h⁻¹. Also included are simulated curves assuming low- and high-temperature reaction routes. Reprinted with permission from *J. Am. Chem. Soc.*, **2017**, *139*, 4935–4942. Copyright 2017, American Chemical Society.

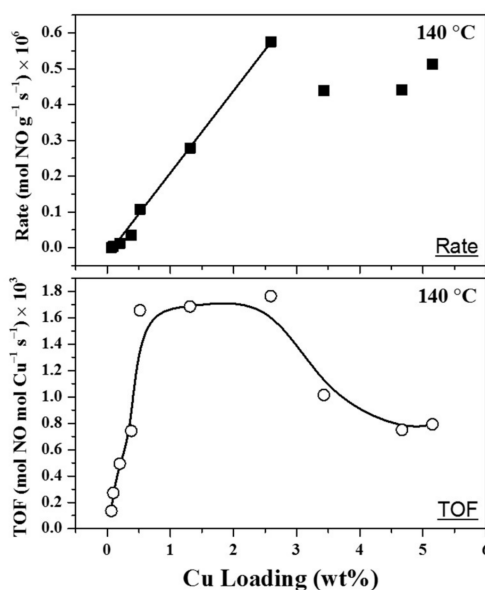


Figure 11. SCR rates (upper panel) and SCR turnover frequencies (lower panel) as a function of Cu loading at a reaction temperature of 140 °C (a temperature used to readily obtain intrinsic, low-conversion reaction kinetics). The reactant feed contains 350 ppm NO, 350 ppm NH₃, 14% O₂, 2.5% H₂O balanced with N₂ at a GHSV of 400,000 h⁻¹. Reprinted from *J. Catal.*, **2014**, *319*, 1–14. Copyright 2014, with permission from Elsevier.

Of special note is that reaction rates at low temperatures are limited by O₂ activation; notably, for the process by which Cu(I) is re-oxidized back to Cu(II) to finish redox cycling of the active sites [19,21]. In particular, a few important experimental findings led to the surprising proposal that rate-limiting, low-temperature O₂ activation requires participation of two Cu(I) sites. First, as shown in Figure 12, for reaction temperatures up to 250 °C, instead of a linear SCR rate versus Cu loading correlation, an interesting linear SCR rate versus (Cu loading)² correlation was discovered by Gao et al. [38], strongly suggesting that the reaction rate limiting step involves participation of

two Cu ions. This surprising experimental result was later reproduced by Gounder, Ribeiro and coworkers [21]. Secondly, in a study on dry NO oxidation to NO₂ by Cu/SSZ-13, Ribeiro and coworkers discovered that isolated Cu ions do not catalyze this reaction, whereas Cu_xO_y (x ≥ 2) clusters contribute linearly to the rate of NO oxidation per mole Cu at 300 °C [46]. This again suggests that only multinuclear Cu species are capable of activating O₂ at low to moderate temperatures. Thirdly, a linear rate versus (Cu loading)² correlation was also found for low-temperature NH₃ oxidation (4NH₃ + 3O₂ = 2N₂ + 6H₂O) [38], suggesting that key intermediates that are associated with the rate-limiting step must contain NH₃ ligands, the common species in both SCR and NH₃ oxidation that, as discussed above, binds with Cu stronger than any other relevant reactants.

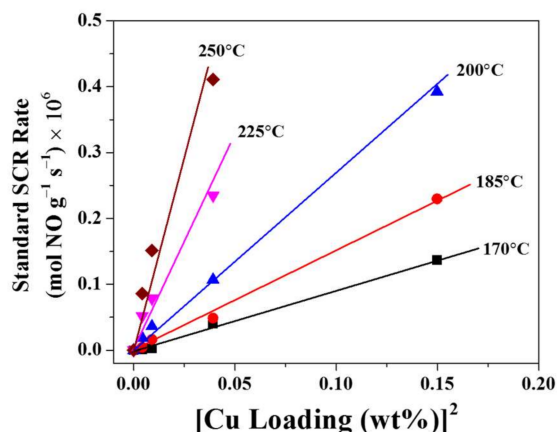
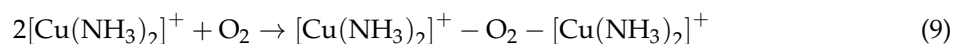


Figure 12. Standard SCR rates (moles NO g⁻¹ s⁻¹) as a function of the square of the Cu loading for reaction on Cu/SSZ-13 catalysts with low Cu loadings. The reactant feed contains 350 ppm NO, 350 ppm NH₃, 14% O₂, 2.5% H₂O balanced with N₂ at a GHSV of 400,000 h⁻¹. Reprinted from *J. Catal.*, 2014, 319, 1–14. Copyright 2014, with permission from Elsevier.

The experimental findings just discussed strongly implicate two NH₃-ligated Cu(I) species collectively in the activation of O₂ as an essential step for standard NH₃-SCR. Assuming that no more than one Cu ion is present in any Chabazite cage (which is indeed the prevalent scenario), migration of such Cu(I) moieties across shared 8 MR windows between neighboring unit cells therefore becomes essential. The realization that linear [Cu(NH₃)₂]⁺ is the most stable and most mobile Cu(I) ion complex makes this species the best candidate for O₂ activation. Based on this, Gao et al. [19] used DFT computer simulations to first propose the following pathway as an essential elemental step for the O₂ activation, that is, the oxidation half-cycle of SCR:



Concurrently, Paolucci, et al. identified this same process as the rate-limiting step for SCR at low temperatures. This group's subsequent Science paper [21] provided many additional important details on the rates of complexed Cu-ion transport and the formation of the binuclear Cu complex. Significantly, Reaction (9) and especially the [Cu(NH₃)₂]⁺ diffusion and Cu-O₂-Cu binding steps, have been proven to be thermodynamically feasible from theoretical simulations [19,21]. At the lowest Cu loadings, formation of the Cu-O₂-Cu intermediate is the rate-limiting, essentially controlled by the entropy costly diffusion of [Cu(NH₃)₂]⁺. Furthermore, low-temperature SCR kinetics measured under such conditions show strong characteristics of mass-transfer limited reaction, with low pre-exponential factors and apparent activation energies [19]. At somewhat higher Cu loadings where 'encounters' of two complexes become more facile and frequent, diffusion of [Cu(NH₃)₂]⁺ and the corresponding activation of O₂, is no longer rate limiting. As a result, all isolated Cu ions become catalytically equivalent, as reflected by the onset of the TOF invariant regime at intermediate Cu loadings (Figure 11).

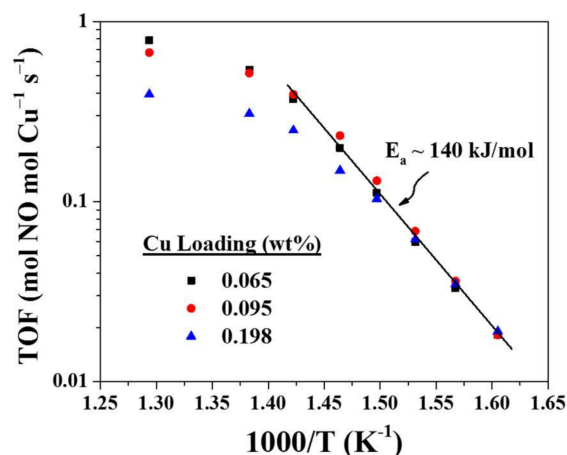
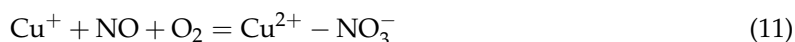
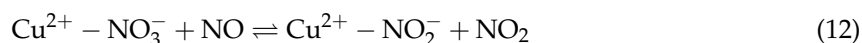


Figure 14. Turnover frequencies (TOFs, mol NO mol Cu⁻¹ s⁻¹) as a function of temperature in Arrhenius plots for low Cu loaded Cu/SSZ-13 (Si/Al = 6). The reactant feed contains 350 ppm NO, 350 ppm NH₃, 14% O₂, 2.5% H₂O balanced with N₂ at a GHSV of 1,200,000 h⁻¹. Different symbols represent samples with different Cu loadings. Reprinted from *J. Catal.*, 2014, 319, 1–14. Copyright 2014, with permission from Elsevier.

Recent operando XAS studies by Lomachenko et al. [15] demonstrate that, above 300 °C, mobile Cu components quickly diminish and four coordinated Cu(II) complexes convert to 3 coordinated ones that spectroscopically resemble a [Cu(II)-NO₃⁻]-Z species. This finding may be used to justify an SCR mechanism proposed by Janssens et al. [13], who postulated that Cu(I) oxidation to Cu(II) is achieved by nitrate intermediate formation from NO+O₂ as the rate-limiting step:

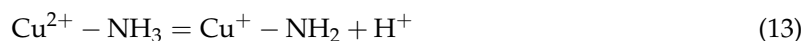


Even though these authors did not specify a temperature window for this mechanism proposal, from our current understanding as discussed above, such a mechanism is clearly not suitable to describe the SCR reaction in the low-temperature regime for the following reasons: (1) it is inconsistent with the Cu loading dependent kinetics found at low temperatures; and (2) Cu ions are heavily ligated with NH₃ in the low temperature regime. According to a very recent operando XAS study by Marberger et al. [26], Cu nitrate species appear only when NH₃ is not readily available; that is, away from SCR conditions. However, at elevated (>300 °C) reaction temperatures, there are currently no experimental findings that disprove this proposal. Nitrate, however, does not interact with NH₃ to form intermediates that directly leads to N₂ + H₂O formation due to a mismatch in charge transfer; that is, the N atom in NO₃⁻ has an oxidation state of +5 while the N atom in NH₃ has an oxidation state of -3. Thus, it is necessary to generate intermediates with an N oxidation state of +3 for a viable mechanism. In the proposal by Janssens et al. [13], this is achieved by the following reaction:



Upon nitrite formation, NH₃ can then interact with it to form an NH₄NO₂ intermediate, which is highly unstable and decomposes selectively to N₂ and H₂O.

Alternatively, high-temperature SCR may follow an Eley-Rideal type of mechanism involving activation of chemisorbed NH₃ as the rate-limiting step. In this case, NH₃ is activated first via an N-H bond cleavage:

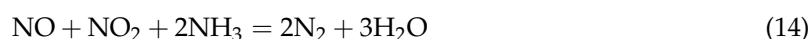


Following Reaction (13), gas-phase NO could interact with the resulting species to form a highly unstable nitrosoamide intermediate (NH₂NO), which also decomposes selectively to N₂ and H₂O.

Note that in these two possible mechanisms, both the nitrate formation and N–H cleavage steps are energetically rather demanding, with DFT-calculated activation energies of ~104 kJ/mol [13] and ~119 kJ/mol [11], respectively. These values are in reasonable agreement with the apparent activation energy of ~140 kJ/mol found experimentally (Figure 14), suggesting that the rate-limiting steps described above are rather plausible. However, more experimental and theoretical studies are certainly needed for a more detailed understanding of the standard SCR mechanism at elevated temperatures.

3.2. Fast NH₃-SCR

The so-called “fast” SCR reaction, occurring when NO_x is composed of both NO and NO₂ ideally in equal amounts, is described by the following stoichiometry [47]:



Despite extensive recent research efforts on Cu/SSZ-13 catalysts, detailed kinetics studies about the fast SCR (Reaction (14)) on this catalyst are surprisingly scarce. There are obvious experimental difficulties: (1) the accumulation of NH₄NO₃ at low reaction temperatures poisons the catalyst and prevents steady-state measurements; (2) high SCR reaction rates at elevated temperatures generally preclude low conversion kinetic measurements; and (3) background reactivity of the SSZ-13 support itself. For example, at reaction temperatures above ~350 °C, fast SCR can proceed so readily on H/SSZ-13 that the presence of Cu has little influence on NO_x conversions [6]. While recent studies by Li et al. [48] of fast SCR mechanisms for H/SSZ-13, using both experimental and theoretical approaches are outside the scope of this review, clearly it is the understanding of lower temperature fast SCR mechanisms on Cu that is of higher significance.

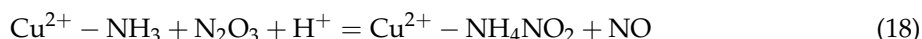
In the low temperature regime, fast SCR most certainly occurs on NH₃-ligated Cu sites. In situ XAS measurements demonstrate that, unlike standard SCR where Cu(II) and Cu(I) coexist, Cu(II) is the only observed Cu oxidation state under fast SCR reaction conditions [34]. This does not at all necessarily mean that Cu(I)/Cu(II) redox cycling is not involved in fast SCR; instead, this result likely indicates that Cu(I) species are extremely short-lived under fast SCR conditions. Indeed, recent studies postulate that NO₂ oxidants accelerate SCR rates both by enhancing Cu(I) oxidation kinetics and by engaging a larger fraction of Cu sites in the catalyst [13,21]. However, to our knowledge, there has not been strong experimental evidence to suggest that fast SCR proceeds at higher rates than standard SCR over Cu/SSZ-13. Indeed, for the isostructural Cu/SAPO-34 catalyst, NO₂ was even found to inhibit low-temperature activity due to NH₄NO₃ poisoning [49]. It can be postulated that this poisoning effect is particularly severe for small pore Cu/Chabazite since pore plugging is clearly more facile in comparison to zeolites with larger pore openings.

With the rather limited kinetics and spectroscopic data available, fast SCR mechanisms for Cu/SSZ-13 can only be speculated about. We note, therefore, that the discussions that follow should not be treated as affirmative but rather suggestive, aiming to encourage more research to fully understand this chemistry. In constructing plausible reaction paths, the following considerations are either established or assumed: (1) active Cu(II) sites at lower reaction temperatures are isolated and they are ligated with NH₃; (2) active NO_x species must have an N oxidation state of +3; (3) intermediates that lead to N₂ and H₂O formation are either nitrosoamide (NH₂NO) or ammonium nitrite (NH₄NO₂), which are known to be highly unstable and decompose readily to the target products; (4) Cu(I) sites are re-oxidized back to the active Cu(II) form by NO₂; and (5) NH₄NO₃ acts as a major side product, poisoning the fast SCR reaction at lower temperatures.

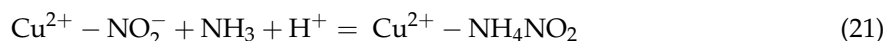
Depending on whether or not the formation of the active NO_x species with an N oxidation state of +3 requires participation of Cu(II), two scenarios are possible. Without Cu(II) participation for charge transfer, NO can be activated by NO₂ to form N₂O₃ non-catalytically, with subsequent interaction of N⁺³ cation species with NH₃-ligated Cu(II) to form intermediates that lead to N₂ + H₂O. The following reaction pathways summarize this first scenario:



In these reactions, since no charge transfer occurs between Cu and NO_x , the role of Cu(II) is to provide a reactive form of NH_3 and to provide a location for the formation of reaction intermediates. Note that Reactions (15–17) are, again, only hypothetical and likely incomplete. Other processes, for example direct $\text{NH}_3 + \text{N}_2\text{O}_3$ reactions, are also possible:



In contrast to the above, if charge transfer between Cu(II) and NO_x does occur (i.e., fast SCR follows a redox mechanism as does standard SCR), then a reduction half-cycle similar to that for standard SCR is also applicable here [11,13]. In particular, a possible second fast SCR mechanism is as follows:



In this case, NO is activated by Cu(II) via formation of a NH_2NO intermediate and Cu(I) is re-oxidized by NO_2 to complete redox cycling.

As noted above, it is not yet clear whether low-temperature fast SCR follows a redox mechanism or not. The lack of observable Cu(I) species under fast SCR conditions may either be due to their non-existence or transient nature. As such, more research is required to elucidate further details of this chemistry. It is clear, though, that side reactions do occur from NO_2 disproportionation that render fast SCR on Cu/SSZ-13 not any faster than standard SCR. In particular, these reactions are described as follows:



Note that H_2O can participate in these latter reactions, in which case HNO_3 and HONO will form as intermediates [50]. However, this will not alter the final product formed, NH_4NO_3 . In fact, NH_4NO_3 has been found to be particularly stable on Cu/SSZ-13, thus displaying a considerable low-temperature inhibition of SCR by blocking pores and channels of the small-pore support [51].

To summarize, in comparison to higher temperature reaction with H/SSZ-13, low-temperature fast SCR is certainly enhanced by the presence of Cu [6]. However, the precise roles that Cu ions play in this reaction is not clear at present. Whether Cu ions actively participate in NO activation (partial oxidation), or they simply provide locations for certain reaction steps to occur, still awaits further study.

4. Towards Rational Design of Cu/SSZ-13

In the above discussions, we have described the current understanding of various transformations of Cu in Cu/SSZ-13 catalysts during synthesis and during SCR reaction. In particular, we have summarized how the roles of these various Cu species in the mechanistic processes that are central to the catalytic chemistry. With this understanding, it becomes possible to suggest catalyst compositions, catalyst processing procedures and reaction conditions for optimum SCR performance. Furthermore, as will be discussed below, Cu speciation can have a profound effect on the stability of Cu/SSZ-13 catalysts. With this in mind, this last section summarizes recent studies that have: (1) determined the known routes for the degradation of Cu/SSZ-13 catalysts; (2) identified undesirable forms of Cu

for long-term catalyst stability and possible mechanistic routes for degrading catalyst performance; and (3) suggested 'design rules' for selecting and synthesizing optimum Cu/SSZ-13 catalysts.

Two major degradation mechanisms have recently been identified for Cu/SSZ-13 SCR catalysts: hydrothermal aging and sulfur poisoning [16]. Sulfur poisoning is typically reversible; adsorbed sulfur (mainly in the form of sulfate) can be removed during high-temperature regeneration treatments. In contrast, hydrothermal degradation is typically irreversible due to permanent structural changes in the zeolite that result in, for example, loss of Brønsted acid sites and changes to the chemical or physical structure of Cu active centers. This explains why hydrothermal aging effects have been so extensively studied [39–41,52–54]. Prior studies have suggested that Cu/SSZ-13 durability enhancement can be achieved in a number of ways: (1) composition optimization, that is, choosing optimized Si/Al and Cu/Al ratios [31]; (2) zeolite particle size optimization [55]; (3) new synthesis methods development [30,56–59]; and (4) introduction of stability enhancement additives. Among these, some appear not to be as useful as others. For example, although it is generally believed that larger zeolite particle size leads to better hydrothermal stability, the study by Proding et al. [55] demonstrates that Cu/SSZ-13 with sub-micrometer particle size does not display inferior hydrothermal stability than Cu/SSZ-13 with particle sizes ~10 times higher. From our own experience, too large of a particle size can even be detrimental due to poor heat dissipation during structure directing agent (SDA) combustion that induces rather serious thermal degradation of the SSZ-13 substrate. Also, new Cu/SSZ-13 synthesis methods, including one-pot ones, do not necessarily lead to catalysts with better stability than catalysts prepared with more traditional solution ion-exchange methods [30,56–59].

In terms of Si/Al ratios, we note that this parameter has changed from ~17.5 for the first generation commercial (BASF) catalyst [40], to ~9.0 for the current state-of-the-art material [16,18]. This change is nontrivial; as suggested by Figure 2, a lower Si/Al ratio allows for a higher percentage of Cu²⁺-2Z sites at similar Cu loadings, thus reducing the formation of undesired CuO_x clusters during hydrothermal aging. As judged from our Cu/SSZ-13 materials synthesized in-house, lowering Si/Al ratios further to ~6 does not lead to catalysts with inferior hydrothermal stability in comparison to catalysts with higher Si/Al ratios, as long as Cu/Al ratios are properly adjusted (more details will be given below). However, very high Si/Al ratios (e.g., 36) are clearly detrimental to hydrothermal stabilities. Therefore, the suggested Si/Al ratios should fall in the range of 6–10 based on our current understanding.

Once Si/Al ratios for an SSZ-13 material is fixed, the most important parameter that influences stability of the final Cu/SSZ-13 product is Cu content, that is, the Cu/Al ratio. Intuitively, one might expect that a full Cu exchange, where all zeolite ion-exchange sites are occupied by Cu ions, best prevents zeolite dealumination and structural degradation. However, even in the very first hydrothermal stability testing of this catalyst, Lobo and coworkers already realized that high Cu/Al ratios are actually detrimental to hydrothermal stability [29]. In particular, as shown in Figure 15 for both Cu/SSZ-13 and Cu/SSZ-16, increasing Cu loading from intermediate to high levels invariably leads to decreased catalytic performance for aged catalysts. These initial results were later fully reproduced by Nam and coworkers, with their XRD measurements demonstrating severe structural damage for highly Cu-loaded catalysts following hydrothermal aging [41]. Two explanations seem possible: (1) somewhat non-intuitively, high Cu loadings induce a high degree of dealumination that destabilizes the SSZ-13 substrate; or (2) as suggested by Lobo and coworkers, copper aluminate and/or copper oxide species are formed during hydrothermal aging that perhaps catalyze the zeolite structure collapse [29].

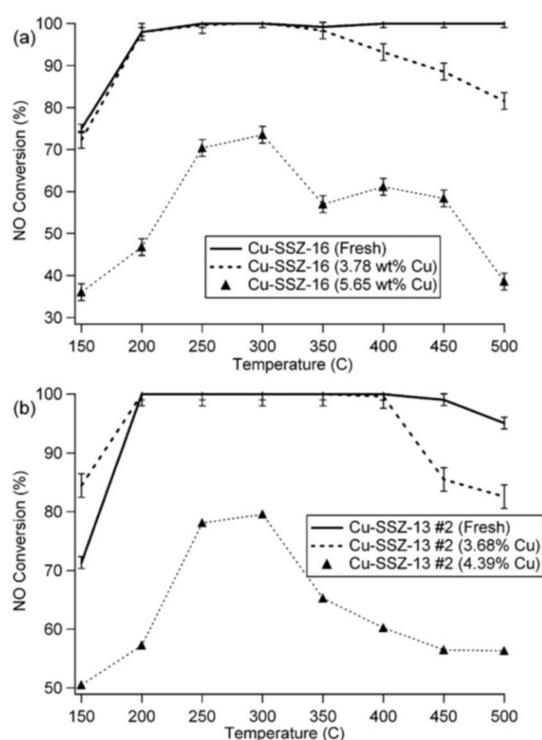


Figure 15. Comparing the effect of copper loading on the NH_3 -SCR activity and hydrothermal stability for (a) Cu-SSZ-16 and (b) Cu-SSZ-13. Reprinted from *Appl. Catal. B-Environ.*, **2011**, *102*, 441–448. Copyright 2011, with permission from Elsevier.

In a recent study of Fe/SSZ-13 catalysts, Kovarik et al. demonstrated that, even with ~80% of dealumination during hydrothermal aging as determined from ^{27}Al NMR quantification, XRD patterns and surface area/pore volume measurements do not show measurable differences in comparison to a fresh catalyst [60]. This strongly suggests that dealumination is not necessarily the primary cause of structural degradation for SSZ-13. A likely explanation is that, unlike many zeolite materials that are only stable within a small range of Si/Al ratios, SSZ-13 is stable at Si/Al from 1 to infinity. In contrast, it is demonstrated below that CuOx clusters formed during hydrothermal aging are more likely to be responsible for structural damage.

Figure 16 compares micro and mesopore size distributions of a Cu/SSZ-13 catalyst with Si/Al = 12 and Cu/Al = 0.25 (the same catalyst used for EPR studies shown in Figure 6) in fresh and two hydrothermally aged (at 700 and 800 °C) forms. These results demonstrate that hydrothermal aging induces no change in micropore size; however, it does cause mesopore formation. For the sample aged at 800 °C in particular, the amount of mesopores that are ≤ 4 nm increases significantly, largely from micropore damage. It is important to note that both hydrothermally aged catalysts have similar extents of dealumination, yet contain increasing amounts of CuOx species relative to the fresh catalyst (Figure 6), likely rationalizing enhanced mesopore formation. Accumulation of such mesopores eventually leads to structural instability and even collapse. It can be expected that such a process depends on temperature, aging time and Cu loading, where higher aging temperatures, longer aging durations and higher Cu loadings promote more damage. Prior literature is fully in line with this structure damage mechanism [39–41,53,61]. On the other hand, dealumination alone is apparently much less destructive for this zeolite catalyst.

Identification of CuOx formation as the main cause of structural instability discussed immediately above and the fact that $[\text{Cu}(\text{OH})]^+\text{-Z}$ selectively converts to CuOx during hydrothermal aging (as discussed in Section 2.2 above), allows for an estimation of Cu/Al ratios that would provide optimum hydrothermal stabilities. For catalysts that contain both kinetically stabilized

$[\text{Cu}(\text{OH})]^+-\text{Z}$ and available 2Al “empty” sites, a hydrothermal treatment at relatively low temperatures (i.e., degreening) promotes Reaction (3), which leads to more stable catalysts. An extra benefit for this treatment, is that a mildly aged Cu/SSZ-13 catalyst will be more resistant to sulfur poisoning. Notably, studies by Luo et al. [16] and Epling and coworkers [23] provide strong evidence to demonstrate that $[\text{Cu}(\text{OH})]^+-\text{Z}$ is much more vulnerable than $\text{Cu}^{2+}-2\text{Z}$ toward sulfur poisoning.

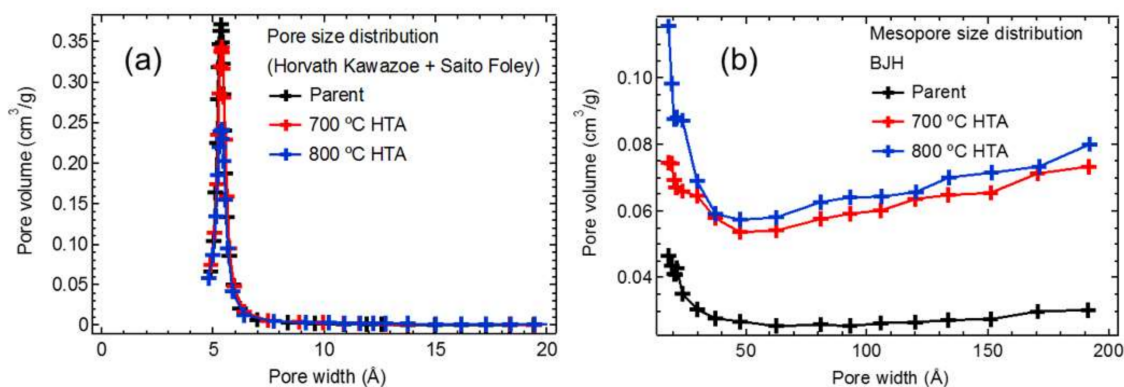


Figure 16. (a) Micropore size distributions of the fresh, HTA-700 and HTA-800 samples determined with the Horvath-Kawazoe and Saito-Foley methods; (b) Mesopore size distributions of the fresh, HTA-700 and HTA-800 samples determined with the BJH method. Reprinted with permission from *ACS Catal.*, 2017, 7, 8214–8227. Copyright 2017, American Chemical Society.

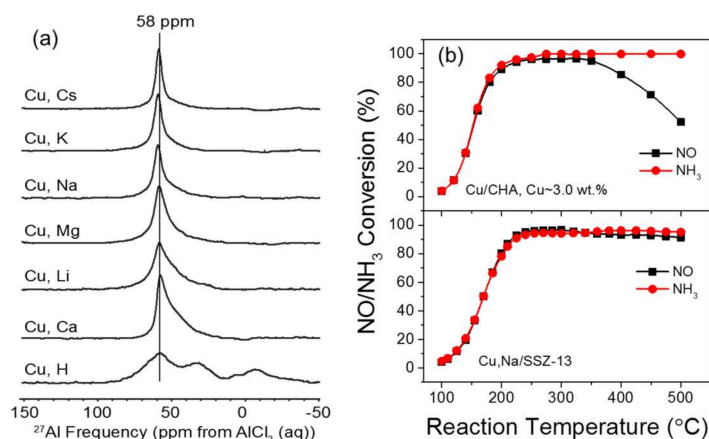


Figure 17. (a) ^{27}Al NMR spectra of hydrothermally aged (HTA) Cu_xH and $\text{Cu}_x\text{M}/\text{SSZ-13}$ catalysts, where M represents alkali and alkaline earth coactions; (b) NO and NH_3 light-off curves for standard SCR over an HTA Cu/SSZ-13 catalyst with $\text{Si}/\text{Al} = 12.5$ and 3.0% Cu and an HTA $\text{Cu}_x\text{Na}/\text{SSZ-13}$ catalyst with $\text{Si}/\text{Al} = 6$, 1.0% Cu and 1.8% Na. Adapted with permission from *ACS Catal.*, 2015, 5, 6780–6791. Copyright 2015, American Chemical Society.

CuO_x formed during hydrothermal aging also causes SCR selectivity to decrease because this species does not efficiently catalyze SCR but is instead active in catalyzing the undesirable NH_3 oxidation reaction at temperatures above ~ 300 °C. This problem may be circumvented with low Cu loaded catalysts where the dominance of $\text{Cu}^{2+}-2\text{Z}$ prevents CuO_x formation during hydrothermal aging. However, for SSZ-13 substrates that are not synthesized with optimized stability themselves, a low Cu loaded composition does not alone satisfactorily improve hydrothermal stabilities. In this case, coaction additives can be added to reduce structural degradation from $-\text{Si}-\text{O}(\text{H})-\text{Al}$ -hydrolysis and even dealumination. In a study by Gao et al. [62], a number of alkali and alkaline earth coactions were tested. As shown in Figure 17a, to varying degrees, all of the coaction additives

show positive effects in preventing structural degradation of the SSZ-13 substrate in comparison to the Cu,H/SSZ-13 counterpart. In the latter undoped case, significant framework Al distortion, partial -Si-O(H)-Al-hydrolysis and dealumination are much more severe than other samples as evidenced by the NMR spectral differences. Figure 17b compares SCR selectivities (i.e., differences between NO and NH₃ conversion) for a hydrothermally aged Cu/SSZ-13 with 3% Cu loading and a hydrothermally aged Cu,Na/SSZ-13 with 1% Cu and 1.8% Na loadings. Clearly, above ~350 °C SCR selectivities for the high Cu loaded sample markedly decrease due to the presence of CuO_x, whereas high SCR selectivities maintain at all reaction temperatures for the low Cu-loaded Cu,Na/SSZ-13 sample due to the absence of CuO_x in this hydrothermally aged catalyst. We note that the Cu and Na loadings used here are not optimized; the purpose of this study was to show that the concept of using additives to enhance Cu/SSZ-13 catalyst stability and performance is indeed a valid one.

5. Concluding Remarks

This short review has focused on Cu/SSZ-13 catalysts that are currently commercialized for diesel vehicle NO_x emission control. In particular, our aims have been to summarize exciting recent insights into the nature of the catalytically active Cu species, some of the critical rate-limiting reactions involved in the complex redox-based standard SCR mechanism at typical reaction temperatures and the effects of Cu speciation on catalyst stability with respect to hydrothermal aging and sulfur poisoning. Of note has been the identification of mobile NH₃-complexed, monomeric Cu ions that are active for the NO_x reduction cycle of the redox mechanism. Significantly and unusually, the thus formed Cu⁺-ion complexes subsequently migrate between zeolite cages to form dimeric species that are the critical catalytic structures for O₂ activation, with the latter reaction being an essential rate-limiting process for the re-oxidation of Cu that completes the catalytic cycle. These conclusions were based on highly unusual reaction kinetics observed experimentally several years ago, yet only recently explained via the application of computational simulations. Studies of Cu speciation under various reaction conditions have also provided clear evidence for the undesirable properties of CuO_x clusters for both SCR selectivity (due to promotion of the NH₃ oxidation reaction) and catalyst stability, where recent results demonstrate a possible 'catalytic' role for CuO_x clusters in degrading the zeolite structure. Processes leading to formation of CuO_x and the 'precursor' forms of Cu ions most susceptible to CuO_x formation were described above. Finally, based on these new molecular-level insights, we discussed how such fundamental information can be used to 'design' Cu/SSZ-13 catalysts for optimized performance and stability.

Acknowledgments: The authors gratefully acknowledge the US Department of Energy (DOE), Energy Efficiency and Renewable Energy, Vehicle Technologies Office for the support of this work at Pacific Northwest National Laboratory (PNNL). PNNL is operated for the US DOE by Battelle.

Author Contributions: Both authors contributed equally to the preparation of the review paper.

Conflicts of Interest: The authors declare no conflict of interest.

References

1. Andersen, P.J.; Collier, J.E.; Casci, J.L.; Chen, H.-Y.; Fedeyko, J.M.; Foo, R.K.S.; Rajaram, R.R. Transition metal/zeolite SCR catalysts. International Patent WO/2008/132452, 11 June 2008.
2. Bull, I.; Xue, W.M.; Burk, P.; Boorse, R.S.; Jaglowski, W.M.; Koerner, G.S.; Moini, A.; Patchett, J.A.; Dettling, J.C.; Caudle, M.T. Copper CHA zeolite catalysts. U.S. Patent 7,601,662 B2, 13 October 2009.
3. Bull, I.; Moini, A.; Koerner, G.S.; Patchett, J.A.; Jaglowski, W.M.; Roth, S. Zeolite catalyst with improved NO_x reduction in SCR. U.S. Patent 7,704,475 B2, 27 April 2010.
4. Andersen, P.J.; Chen, H.-Y.; Fedeyko, J.M.; Weigert, E. Small pore molecular sieve supported copper catalysts durable against lean/rich aging for the reduction of nitrogen oxides. U.S. Patent 7,998,443 B2, 16 August 2011.
5. Gao, F.; Kwak, J.H.; Szanyi, J.; Peden, C.H.F. Current understanding of Cu-exchanged Chabazite molecular sieves for use as commercial diesel engine DeNO_x catalysts. *Top. Catal.* **2013**, *56*, 1441–1459. [[CrossRef](#)]

6. Beale, A.M.; Gao, F.; Lezcano-Gonzalez, I.; Peden, C.H.F.; Szanyi, J. Recent advances in automotive catalysis for NO_x emission control by small-pore microporous materials. *Chem. Soc. Rev.* **2015**, *44*, 7371–7405. [[CrossRef](#)] [[PubMed](#)]
7. Paolucci, C.; di Iorio, J.R.; Ribeiro, F.H.; Gounder, R.; Schneider, W.F. Catalysis science of NO_x selective catalytic reduction with ammonia over Cu-SSZ-13 and Cu-SAPO-34. *Adv. Catal.* **2016**, *59*, 1–107.
8. Wang, J.H.; Zhao, H.W.; Haller, G.; Li, Y.D. Recent advances in the selective catalytic reduction of NO_x with NH₃ on Cu-Chabazite catalysts. *Appl. Catal. B Environ.* **2017**, *202*, 346–354. [[CrossRef](#)]
9. Nova, I.; Tronconi, E. *Urea-SCR Technology for deNO_x after Treatment of Diesel Exhausts*; Springer Science & Business Media: New York, NY, USA, 2014.
10. Zones, S.I. Zeolite SSZ-13 and its method of preparation. U.S. Patent 4,544,538, 1 October 1985.
11. Paolucci, C.; Verma, A.A.; Bates, S.A.; Kispersky, V.F.; Miller, J.T.; Gounder, R.; Delgass, W.N.; Ribeiro, F.H.; Schneider, W.F. Isolation of the Copper Redox Steps in the Standard Selective Catalytic Reduction on Cu-SSZ-13. *Angew. Chem. Int. Ed.* **2014**, *53*, 11828–11833. [[CrossRef](#)] [[PubMed](#)]
12. Di Iorio, J.R.; Bates, S.A.; Verma, A.A.; Delgass, W.N.; Ribeiro, F.H.; Miller, J.T.; Gounder, R. The dynamic nature of Brønsted acid sites in Cu-Zeolites during NO_x selective catalytic reduction: Quantification by gas-phase ammonia titration. *Top. Catal.* **2015**, *58*, 424–434. [[CrossRef](#)]
13. Janssens, T.V.W.; Falsig, H.; Lundegaard, L.F.; Vennestrom, P.N.R.; Rasmussen, S.B.; Moses, P.G.; Giordanino, F.; Borfecchia, E.; Lomachenko, K.A.; Lamberti, C.; et al. A consistent reaction scheme for the selective catalytic reduction of nitrogen oxides with ammonia. *ACS Catal.* **2015**, *5*, 2832–2845. [[CrossRef](#)]
14. Moreno-Gonzalez, M.; Hueso, B.; Boronat, M.; Blasco, T.; Corma, A. Ammonia-containing species formed in Cu-Chabazite as per in situ EPR, solid-state NMR and DFT calculations. *J. Phys. Chem. Lett.* **2015**, *6*, 1011–1017. [[CrossRef](#)] [[PubMed](#)]
15. Lomachenko, K.A.; Borfecchia, E.; Negri, C.; Berlier, G.; Lamberti, C.; Beato, P.; Falsig, H.; Bordiga, S. The Cu-CHA deNO_x Catalyst in Action: Temperature-Dependent NH₃-Assisted Selective Catalytic Reduction Monitored by Operando XAS and XES. *J. Am. Chem. Soc.* **2016**, *138*, 12025–12028. [[CrossRef](#)] [[PubMed](#)]
16. Luo, J.Y.; Wang, D.; Kumar, A.; Li, J.H.; Kamasamudram, K.; Currier, N.; Yezerets, A. Identification of two types of Cu sites in Cu/SSZ-13 and their unique responses to hydrothermal aging and sulfur poisoning. *Catal. Today* **2016**, *267*, 3–9. [[CrossRef](#)]
17. Paolucci, C.; Parekh, A.A.; Khurana, I.; Di Iorio, J.R.; Li, H.; Albarracin-Caballero, J.D.; Shih, A.J.; Anggara, T.; Delgass, W.N.; Miller, J.T.; et al. Catalysis in a cage: Condition-dependent speciation and dynamics of exchanged Cu cations in SSZ-13 zeolites. *J. Am. Chem. Soc.* **2016**, *138*, 6028–6048. [[CrossRef](#)] [[PubMed](#)]
18. Luo, J.Y.; Gao, F.; Kamasamudram, K.; Currier, N.; Peden, C.H.F.; Yezerets, A. New insights into Cu/SSZ-13 SCR catalyst acidity. Part I: Nature of acidic sites probed by NH₃ titration. *J. Catal.* **2017**, *348*, 291–299. [[CrossRef](#)]
19. Gao, F.; Mei, D.H.; Wang, Y.L.; Szanyi, J.; Peden, C.H.F. Selective catalytic reduction over Cu/SSZ-13: Linking homo- and heterogeneous catalysis. *J. Am. Chem. Soc.* **2017**, *139*, 4935–4942. [[CrossRef](#)] [[PubMed](#)]
20. Martini, A.; Borfecchia, E.; Lomachenko, K.A.; Pankin, I.A.; Negri, C.; Berlier, G.; Beato, P.; Falsig, H.; Bordiga, S.; Lamberti, C. Composition-driven Cu-speciation and reducibility in Cu-CHA zeolite catalysts: A multivariate XAS/FTIR approach to complexity. *Chem. Sci.* **2017**, *8*, 6836–6851. [[CrossRef](#)] [[PubMed](#)]
21. Paolucci, C.; Khurana, I.; Parekh, A.A.; Li, S.C.; Shih, A.J.; Li, H.; Di Iorio, J.R.; Albarracin-Caballero, J.D.; Yezerets, A.; Miller, J.T.; et al. Dynamic multinuclear sites formed by mobilized copper ions in NO_x selective catalytic reduction. *Science* **2017**, *357*, 898–903. [[CrossRef](#)] [[PubMed](#)]
22. Schmidt, J.E.; Oord, R.; Guo, W.; Poplawsky, J.D.; Weckhuysen, B.M. Nanoscale tomography reveals the deactivation of automotive copper-exchanged zeolite catalysts. *Nat. Commun.* **2017**, *8*. [[CrossRef](#)]
23. Jangjou, Y.; Do, Q.; Gu, Y.T.; Lim, L.-G.; Sun, H.; Wang, D.; Kumar, A.; Li, J.H.; Grabow, L.C.; Epling, W.S. On the nature of Cu active centers in Cu-SSZ-13 and their responses to SO₂ exposure. *ACS Catal.* **2018**, *8*, 1325–1337. [[CrossRef](#)]
24. Godiksen, A.; Isaksen, O.L.; Rasmussen, S.B.; Vennestrom, P.N.R.; Mossin, S. Site-Specific Reactivity of Copper Chabazite Zeolites with Nitric Oxide, Ammonia and Oxygen. *ChemCatChem* **2018**, *10*, 366–370. [[CrossRef](#)]
25. Andersen, C.W.; Borfecchia, E.; Bremholm, M.; Jorgensen, M.R.V.; Vennestrom, P.N.R.; Lamberti, C.; Lundegaard, L.F.; Iversen, B.B. Redox-Driven Migration of Copper Ions in the Cu-CHA Zeolite as Shown by the In Situ PXRD/XANES Technique. *Angew. Chem. Int. Ed.* **2017**, *56*, 10367–10372. [[CrossRef](#)] [[PubMed](#)]
26. Marberger, A.; Petrov, A.W.; Steiger, P.; Elsener, M.; Kröcher, O.; Nachttegaal, M.; Ferri, D. Time-resolved copper speciation during selective catalytic reduction of NO on Cu-SSZ-13. *Nat. Catal.* **2018**, *1*, 221–227. [[CrossRef](#)]

27. Fickel, D.W.; Lobo, R.F. Copper coordination in Cu-SSZ-13 and Cu-SSZ-16 investigated by variable-temperature XRD. *J. Phys. Chem. C* **2010**, *114*, 1633–1640. [[CrossRef](#)]
28. Kwak, J.H.; Tonkyn, R.G.; Kim, D.H.; Szanyi, J.; Peden, C.H.F. Excellent activity and selectivity of Cu-SSZ-13 in the selective catalytic reduction of NO_x with NH₃. *J. Catal.* **2010**, *275*, 187–190. [[CrossRef](#)]
29. Fickel, D.W.; D'Addio, E.; Lauterbach, J.A.; Lobo, R.F. The ammonia selective catalytic reduction activity of copper-exchanged small-pore zeolites. *Appl. Catal. B Environ.* **2011**, *102*, 441–448. [[CrossRef](#)]
30. Ren, L.M.; Zhu, L.F.; Yang, C.G.; Chen, Y.M.; Sun, Q.; Zhang, H.Y.; Li, C.J.; Nawaz, F.; Meng, X.J.; Xiao, F.S. Designed copper–amine complex as an efficient template for one-pot synthesis of Cu-SSZ-13 zeolite with excellent activity for selective catalytic reduction of NO_x by NH₃. *Chem. Commun.* **2011**, *47*, 9789–9791. [[CrossRef](#)] [[PubMed](#)]
31. Gao, F.; Washton, N.M.; Wang, Y.L.; Kollar, M.; Szanyi, J.; Peden, C.H.F. Effects of Si/Al ratio on Cu/SSZ-13 NH₃-SCR catalysts: Implications for the active Cu species and the roles of Brønsted acidity. *J. Catal.* **2015**, *331*, 25–38. [[CrossRef](#)]
32. Kwak, J.H.; Zhu, H.Y.; Lee, J.H.; Peden, C.H.F.; Szanyi, J. Two different cationic positions in Cu-SSZ-13? *Chem. Commun.* **2012**, *48*, 4758–4760. [[CrossRef](#)] [[PubMed](#)]
33. Andersen, C.W.; Bremholm, M.; Vennestrom, P.N.R.; Blichfeld, A.B.; Lundegaard, L.F.; Iversen, B.B. Location of Cu²⁺ in CHA zeolite investigated by X-ray diffraction using the Rietveld/maximum entropy method. *IUCr* **2014**, *1*, 382–386. [[CrossRef](#)] [[PubMed](#)]
34. McEwen, J.S.; Anggara, T.; Schneider, W.F.; Kispersky, V.F.; Miller, J.T.; Delgass, W.N.; Ribeiro, F.H. Integrated operando X-ray absorption and DFT characterization of Cu-SSZ-13 exchange sites during the selective catalytic reduction of NO_x with NH₃. *Catal. Today* **2012**, *184*, 129–144. [[CrossRef](#)]
35. Kwak, J.H.; Varga, T.; Peden, C.H.F.; Gao, F.; Hanson, J.C.; Szanyi, J. Following the movement of Cu ions in a SSZ-13 zeolite during dehydration, reduction and adsorption: A combined in situ TP-XRD, XANES/DRIFTS study. *J. Catal.* **2014**, *314*, 83–93. [[CrossRef](#)]
36. Godiksen, A.; Stappen, F.N.; Vennestrom, P.N.R.; Giordanino, F.; Rasmussen, S.B.; Lundegaard, L.F.; Mossin, S. Coordination environment of copper sites in Cu-CHA zeolite investigated by electron paramagnetic resonance. *J. Phys. Chem. C* **2014**, *118*, 23126–23138. [[CrossRef](#)]
37. Song, J.; Wang, Y.L.; Walter, E.D.; Washton, N.M.; Mei, D.H.; Kovarik, L.; Engelhard, M.H.; Proding, S.; Wang, Y.; Peden, C.H.F.; Gao, F. Toward Rational Design of Cu/SSZ-13 Selective Catalytic Reduction Catalysts: Implications from Atomic-Level Understanding of Hydrothermal Stability. *ACS Catal.* **2017**, *7*, 8214–8227. [[CrossRef](#)]
38. Gao, F.; Walter, E.D.; Kollar, M.; Wang, Y.L.; Szanyi, J.; Peden, C.H.F. Understanding ammonia selective catalytic reduction kinetics over Cu/SSZ-13 from motion of the Cu ions. *J. Catal.* **2014**, *319*, 1–14. [[CrossRef](#)]
39. Kwak, J.H.; Tran, D.; Burton, S.D.; Szanyi, J.; Lee, J.H.; Peden, C.H.F. Effects of hydrothermal aging on NH₃-SCR reaction over Cu/zeolites. *J. Catal.* **2012**, *287*, 203–209. [[CrossRef](#)]
40. Schmieg, S.J.; Oh, S.H.; Kim, C.H.; Brown, D.B.; Lee, J.H.; Peden, C.H.F.; Kim, D.H. Thermal durability of Cu-CHA NH₃-SCR catalysts for diesel NO_x reduction. *Catal. Today* **2012**, *184*, 252–261. [[CrossRef](#)]
41. Kim, Y.J.; Lee, J.K.; Min, K.M.; Hong, S.B.; Nam, I.S.; Cho, B.K. Hydrothermal stability of CuSSZ13 for reducing NO_x by NH₃. *J. Catal.* **2014**, *311*, 447–457. [[CrossRef](#)]
42. Vennestrom, P.N.R.; Janssens, T.V.W.; Kustov, A.; Grill, M.; Puig-Molina, A.; Lundegaard, L.F.; Tiruvalam, R.R.; Concepcion, P.; Corma, A. Influence of lattice stability on hydrothermal deactivation of Cu-ZSM-5 and Cu-IM-5 zeolites for selective catalytic reduction of NO_x by NH₃. *J. Catal.* **2014**, *309*, 477–490. [[CrossRef](#)]
43. Giordanino, F.; Borfecchia, E.; Lomachenko, K.A.; Lazzarini, A.; Agostini, G.; Gallo, E.; Soldatov, A.V.; Beato, P.; Bordiga, S.; Lamberti, C. Interaction of NH₃ with Cu-SSZ-13 catalyst: A complementary FTIR, XANES and XES study. *J. Phys. Chem. Lett.* **2014**, *5*, 1552–1559. [[CrossRef](#)] [[PubMed](#)]
44. Shwan, S.; Skoglundh, M.; Lundegaard, L.F.; Tiruvalam, R.R.; Janssens, T.V.W.; Carlsson, A.; Vennestrom, P.N.R. Solid-state ion-exchange of copper into zeolites facilitated by ammonia at low temperature. *ACS Catal.* **2015**, *5*, 16–19. [[CrossRef](#)]
45. Clemens, A.K.S.; Shishkin, A.; Carlsson, P.A.; Skoglundh, M.; Martinez-Casado, F.J.; Matej, Z.; Balmes, O.; Harelind, H. Reaction-driven ion exchange of copper into zeolite SSZ-13. *ACS Catal.* **2015**, *5*, 6209–6218. [[CrossRef](#)]

46. Verma, A.A.; Bates, S.A.; Anggara, T.; Paolucci, C.; Parekh, A.A.; Kamasamudram, K.; Yezerets, A.; Miller, J.T.; Delgass, W.N.; Schneider, W.F.; Ribeiro, F.H. NO oxidation: A probe reaction on Cu-SSZ-13. *J. Catal.* **2014**, *312*, 179–190. [[CrossRef](#)]
47. Brandenberger, S.; Krocher, O.; Tissler, A.; Althoff, R. The state of the art in selective catalytic reduction of NO_x by Ammonia using metal-exchanged zeolite catalysts. *Catal. Rev. Sci. Eng.* **2008**, *50*, 492–531. [[CrossRef](#)]
48. Li, S.C.; Zheng, Y.; Gao, F.; Szanyi, J.; Schneider, W.F. Experimental and Computational Interrogation of Fast SCR Mechanism and Active Sites on H-Form SSZ-13. *ACS Catal.* **2017**, *7*, 5087–5096. [[CrossRef](#)]
49. Hao, T.; Wang, J.; Yu, T.; Wang, J.Q.; Shen, M.Q. Effect of NO₂ on the Selective Catalytic Reduction of NO with NH₃ over Cu/SAPO-34 Molecular Sieve Catalyst. *Acta Phys. Chim. Sin.* **2014**, *30*, 1567–1574.
50. Gao, F.; Wang, Y.L.; Kollar, M.; Washton, N.M.; Szanyi, J.; Peden, C.H.F. A comparative kinetics study between Cu/SSZ-13 and Fe/SSZ-13 SCR catalysts. *Catal. Today* **2015**, *258*, 347–358. [[CrossRef](#)]
51. Chen, H.-Y.; Wei, Z.H.; Kollar, M.; Gao, F.; Wang, Y.L.; Szanyi, J.; Peden, C.H.F. A comparative study of N₂O formation during the selective catalytic reduction of NO_x with NH₃ on zeolite supported Cu catalysts. *J. Catal.* **2015**, *329*, 490–498. [[CrossRef](#)]
52. Ye, Q.; Wang, L.F.; Yang, R.T. Activity, propene poisoning resistance and hydrothermal stability of copper exchanged Chabazite-like zeolite catalysts for SCR of NO with ammonia in comparison to Cu/ZSM-5. *Appl. Catal. A Gen.* **2012**, *427–428*, 24–34. [[CrossRef](#)]
53. Blakeman, P.G.; Burkholder, E.M.; Chen, H.Y.; Collier, J.E.; Fedeyko, J.M.; Jobson, H.; Rajaram, R.R. The role of pore size on the thermal stability of zeolite supported Cu SCR catalysts. *Catal. Today* **2014**, *231*, 56–63. [[CrossRef](#)]
54. Lezcano-Gonzalez, I.; Deka, U.; van der Bij, H.E.; Paalanen, P.; Arstad, B.; Weckhuysen, B.M.; Beale, A.M. Chemical deactivation of Cu-SSZ-13 ammonia selective catalytic reduction (NH₃-SCR) systems. *Appl. Catal. B Environ.* **2014**, *154–155*, 339–349. [[CrossRef](#)]
55. Prodingler, S.; Derewinski, M.A.; Wang, Y.L.; Washton, N.M.; Walter, E.D.; Szanyi, J.; Gao, F.; Wang, Y.; Peden, C.H.F. Sub-micron Cu/SSZ-13: Synthesis and application as selective catalytic reduction (SCR) catalysts. *Appl. Catal. B Environ.* **2017**, *201*, 461–469. [[CrossRef](#)]
56. Martinez-Franco, R.; Moliner, M.; Thogersen, J.R.; Corma, A. Efficient One-Pot Preparation of Cu-SSZ-13 Materials using Cooperative OSDAs for their Catalytic Application in the SCR of NO_x. *ChemCatChem* **2013**, *5*, 3316–3323. [[CrossRef](#)]
57. Martin, N.; Moliner, M.; Corma, A. High yield synthesis of high-silica Chabazite by combining the role of zeolite precursors and tetraethylammonium: SCR of NO_x. *Chem. Commun.* **2015**, *51*, 9965–9968. [[CrossRef](#)] [[PubMed](#)]
58. Wang, X.; Wu, Q.M.; Chen, C.Y.; Pan, S.X.; Zhang, W.P.; Meng, X.J.; Maurer, S.; Feyen, M.; Muller, U.; Xiao, F.-S. Atom-economical synthesis of a high silica CHA zeolite using a solvent-free route. *Chem. Commun.* **2015**, *51*, 16920–16923. [[CrossRef](#)] [[PubMed](#)]
59. Zhao, Z.C.; Yu, R.; Zhao, R.R.; Shi, C.; Gies, H.; Xiao, F.S.; de Vos, D.; Yokoi, T.; Bao, X.H.; Kolb, U.; et al. Cu-exchanged Al-rich SSZ-13 zeolite from organotemplate-free synthesis as NH₃-SCR catalyst: Effects of Na⁺ ions on the activity and hydrothermal stability. *Appl. Catal. B Environ.* **2017**, *217*, 421–428. [[CrossRef](#)]
60. Kovarik, L.; Washton, N.M.; Kukadapu, R.; Devaraj, A.; Wang, A.Y.; Wang, Y.L.; Szanyi, J.; Peden, C.H.F.; Gao, F. Transformation of active sites in Fe/SSZ-13 SCR catalysts during hydrothermal aging: A spectroscopic, microscopic and kinetics study. *ACS Catal.* **2017**, *7*, 2458–2470. [[CrossRef](#)]
61. Wang, D.; Jangjou, Y.; Liu, Y.; Sharma, M.K.; Luo, J.Y.; Li, J.H.; Kamasamudram, K.; Epling, W.S. A comparison of hydrothermal aging effects on NH₃-SCR of NO_x over Cu-SSZ-13 and Cu-SAPO-34 catalysts. *Appl. Catal. B Environ.* **2015**, *165*, 438–445. [[CrossRef](#)]
62. Gao, F.; Wang, Y.L.; Washton, N.M.; Kollar, M.; Szanyi, J.; Peden, C.H.F. Effects of alkali and alkaline earth cocations on the activity and hydrothermal stability of Cu/SSZ-13 NH₃-SCR catalysts. *ACS Catal.* **2015**, *5*, 6780–6791. [[CrossRef](#)]

